Lab on a Chip

PAPER

View Article Online
View Journal | View Issue

Open Access Article. Published on 09 June 2015. Downloaded on 7/25/2025 4:28:56 AM.
This article is licensed under a Creative Commons Attribution-NonCommercial 3.0 Unported Licence.

CrossMark click for updates

Cite this: *Lab Chip*, 2015, **15**, 3047

Photopatterned oil-reservoir micromodels with tailored wetting properties†

Hyundo Lee,[a] Seung Goo Lee[b] and Patrick S. Doyle*[b]

Received 9th March 2015,
Accepted 8th June 2015

DOI: 10.1039/c5lc00277j

www.rsc.org/loc

Micromodels with a simplified porous network that represents geological porous media have been used as experimental test beds for multiphase flow studies in the petroleum industry. We present a new method to fabricate reservoir micromodels with heterogeneous wetting properties. Photopatterned, copolymerized microstructures were fabricated in a bottom-up manner. The use of rationally designed copolymers allowed us to tailor the wetting behavior (oleophilic/phobic) of the structures without requiring additional surface modifications. Using this approach, two separate techniques of constructing microstructures and tailoring their wetting behavior are combined in a simple, single-step ultraviolet lithography process. This microstructuring method is fast, economical, and versatile compared with previous fabrication methods used for multi-phase micromodel experiments. The wetting behaviors of the copolymerized microstructures were quantified and demonstrative oil/water immiscible displacement experiments were conducted.

1 Introduction

It is common practice to use core samples from oil reservoir sites to understand oil–gas–water multiphase flow occurring in underground oil reservoirs.[1–7] However, the disadvantages of core-flooding experiments (*e.g.* opacity, site specificity, ambiguities of experimental parameters) have impeded fundamental investigations of oil reservoirs in the laboratory environment.

Due to such limitations of core-flooding experiments, researchers have recently developed synthetic micromodels using microfabrication techniques. Micromodels are usually two-dimensional and transparent microchannels with a simplified porous network designed to visualize and study fluid behavior in porous media.[8–10] In oil reservoir research, micromodels reflect underground oil reservoir conditions, for example, porosity, permeability, and wettability.[11–14] These reservoir properties are designed and built into micromodels for further understanding of fundamental fluid behavior and interactions among oil–water–rock phases. Micromodel studies in the laboratory environment are required for various real field applications, such as operational practices for oil production, enhanced oil recovery with various materials (surfactant,[15] polymer,[16] foam,[17,18] steam[19]), and reservoir network mapping.[20]

It is estimated that more than 60% of the world's oil and 40% of the world's gas reserves are held in carbonate reservoirs. For example, the Middle East is dominated by carbonate rocks, with around 70% of oil and 90% of gas reserves held within these reservoirs. When it comes to carbonate reservoirs, even though their main component, calcite, inherently shows water-wet behavior, the surface wetting property of carbonate oil reservoir rocks is known to be mostly oil-wet.[21] Treiber *et al.* investigated 50 samples and showed that only 8% of the carbonate reservoir rocks were water-wet, 8% intermediate-wet, and 84% oil-wet.[22] That being said, the pertinent wetting properties of micromodels were not measured or controlled in previous studies. Most prior research only investigated the wettability of micromodels in solid–liquid–air systems, hydro-philicity/phobicity in air or oleo-philicity/phobicity in air. Since both hydrophilic and hydrophobic surfaces might be oleophilic (or oleophobic) in water,[23] it is necessary to investigate the micromodel's wetting preference in the presence of both water and oil.[23–25]

Various fabrication techniques have been employed to build micromodels,[8,9] including plasma etching of silicon,[26] deep reactive ion etching of glass,[27,28] and soft lithography with polymeric materials.[17,29–37] More recently, Song *et al.* developed a real-rock micromodel by wet etching of natural carbonate rock.[38] These fabrication methods are often time consuming and involve access to cleanroom microfabrication facilities which can result in high unit costs for a single micromodel. Moreover, once the design of features or

[a] *Department of Mechanical Engineering, Massachusetts Institute of Technology, Cambridge, MA, 02139, USA*
[b] *Department of Chemical Engineering, Massachusetts Institute of Technology, Cambridge, MA, 02139, USA. E-mail: pdoyle@mit.edu; Fax: +1 617 258 5042; Tel: +1 617 253 4534*

† Electronic supplementary information (ESI) available. See DOI: 10.1039/c5lc00277j

Open Access Article. Published on 09 June 2015. Downloaded on 7/25/2025 4:28:56 AM.
This article is licensed under a Creative Commons Attribution-NonCommercial 3.0 Unported Licence.

patterns are fabricated, it is nearly impossible to make geometric modifications on-the-fly and quickly iterate on designs.

In addition to micromodel fabrication methods, there have been significant advances in methods to modify wetting properties within micromodels to mimic an oil reservoir's wetting features. These approaches include silanization,[39] UV-ozone treatment,[17,40] and UV-initiated polymer grafting.[31,41] However, these approaches to tune wettability also have some limitations. They all require additional post-processing of a device. Furthermore it is well known that an UV-ozone treated PDMS (polydimethylsiloxane) surface recovers its native hydrophobicity by the oligomer migration from the bulk PDMS to the surface.[42,43] Moreover, due to the lack of ability to tune wetting over a continuous range, it is hard to reproduce the complex wetting properties of an oil reservoir having locally different and more than two surface properties. A more detailed comparison of micromodel fabrication and tailored wettability approaches is given in the ESI.† To summarize, the major shortcomings of previous fabrication methods for oil-reservoir micromodels are inflexibility in design and the lack of control in wetting properties.

By adapting the Stop-Flow-Lithography (SFL) technique,[44–46] we have developed a new, versatile, and bottom-up micromodel fabrication technique in which microstructure synthesis and wetting property control are combined in a single lithographic step. Unlike SFL, which is used to create free-standing microparticles, here the top and bottom glass surfaces of microchannels are acrylated, and so the polymerized microstructures adhere to the glass. We demonstrate that quasi-two-dimensional porous structures with defined geometric features and predetermined heterogeneous wetting properties can be polymerized within seconds.

2 Materials and methods

In this work, we utilized the stop-flow-lithography (SFL) technique[45] to construct polymeric structures in initially empty microchannels. SFL introduces streams of precursor with a controlled-pressure pump, stops the flow, then polymerizes microparticles with specific geometric features through predefined transparent masks, and finally releases microparticles with supplying pressure again. This stop-polymerization-flow sequence is repeated, and SFL produces high-resolution microparticles at high throughput. Instead of producing functional microparticles, we utilized this photopatterning technique to build polymeric structures in initially empty microchannels.

2.1 Surface activation for polymeric structure fixation

During the SFL process, polymerized particles are not bound to the top and bottom surfaces due to the oxygen permeability of PDMS (polydimethylsiloxane); thin oxygen layers inhibit the polymerization of precursor solutions near top and bottom surfaces.[47] Since we wanted to build desired structures in microchannels using a bottom-up approach, it was necessary to either control the oxygen environment during polymerization or use gas-impermeable surfaces; we chose the latter. It is also necessary to modify the chemistry of top and bottom surfaces to hold the polymerized structures in place for future use of flow studies. We adapted the following surface activation procedure as previously done by Srinivas *et al.* for fixing PEG-DA (poly(ethylene glycol)diacrylate) hydrogel posts in bioassays.[48]

First an empty glass microfluidic channel (Hilgenberg GmbH, Germany) was filled with 1 M sodium hydroxide aqueous solution for 1 hour. After thoroughly rinsing the microchannel with ethanol and water, the channel was filled with 3-(trimethoxysilyl)propyl acrylate (Sigma-Aldrich) for 5 minutes. The microchannel was thoroughly rinsed with ethanol and water again, and cured at 80 °C for 15 minutes for sufficient reaction. Later, when ultraviolet polymerization reaction occurred, the top and bottom glass surfaces modified with acrylate functional group promoted polymer structure fixation on the surfaces (Fig. 1A).

2.2 Microstructuring by photolithography

With proper ratios of crosslinkers, monomers, and a photoinitiator, hydrophilic and oleophilic structures were built into surface activated glass microchannels. A thoroughly mixed precursor solution was injected into the activated glass–glass channel and UV-polymerization was done on the stage of an inverted microscope (Zeiss Axio Observer A1). A photomask of desired geometric shape was inserted into the field stop of the microscope, and the microchannel was then placed and aligned properly. UV exposure time was controlled by switching a LED light source on and off with LabView. After building microstructures, any uncured precursor solution was washed out of the device with acetone (Fig. 1A).

2.3 Tailoring wetting properties by copolymerization

The displacement of oil with other fluids that exist in reservoirs (*e.g.* gas, brine, water), needs to be considered at the pore scale. When the transport phenomena occur in porous reservoirs, the wetting property is a critical factor and has to be taken into consideration, as well as other geometric features such as porosity and permeability. In this experimental study, we are interested in oil–water flow around geometric structures with tuned wetting properties. As mentioned previously, the relative preference between oil and water has to be precisely defined and investigated in water–oil displacement study to understand displacement process occurring underground oil reservoir. Since the wettability is a relative preference of a solid surface to different fluids, it is prerequisite to have designed wetting preferences of oil-like (oleophilic) and water-like (hydrophilic) depending on the configuration of water contact angle in oil.[49] The concept of hydrophilic/hydrophobic is usually defined in the presence of solid–water–air, however that of oleophilic/oleophobic is inarticulately used, it is used to define the relation of solid–oil–air or solid–water–oil. A common mistake is to assume that a

 This journal is © The Royal Society of Chemistry 2015

Open Access Article. Published on 09 June 2015. Downloaded on 7/25/2025 4:28:56 AM.
This article is licensed under a Creative Commons Attribution-NonCommercial 3.0 Unported Licence.

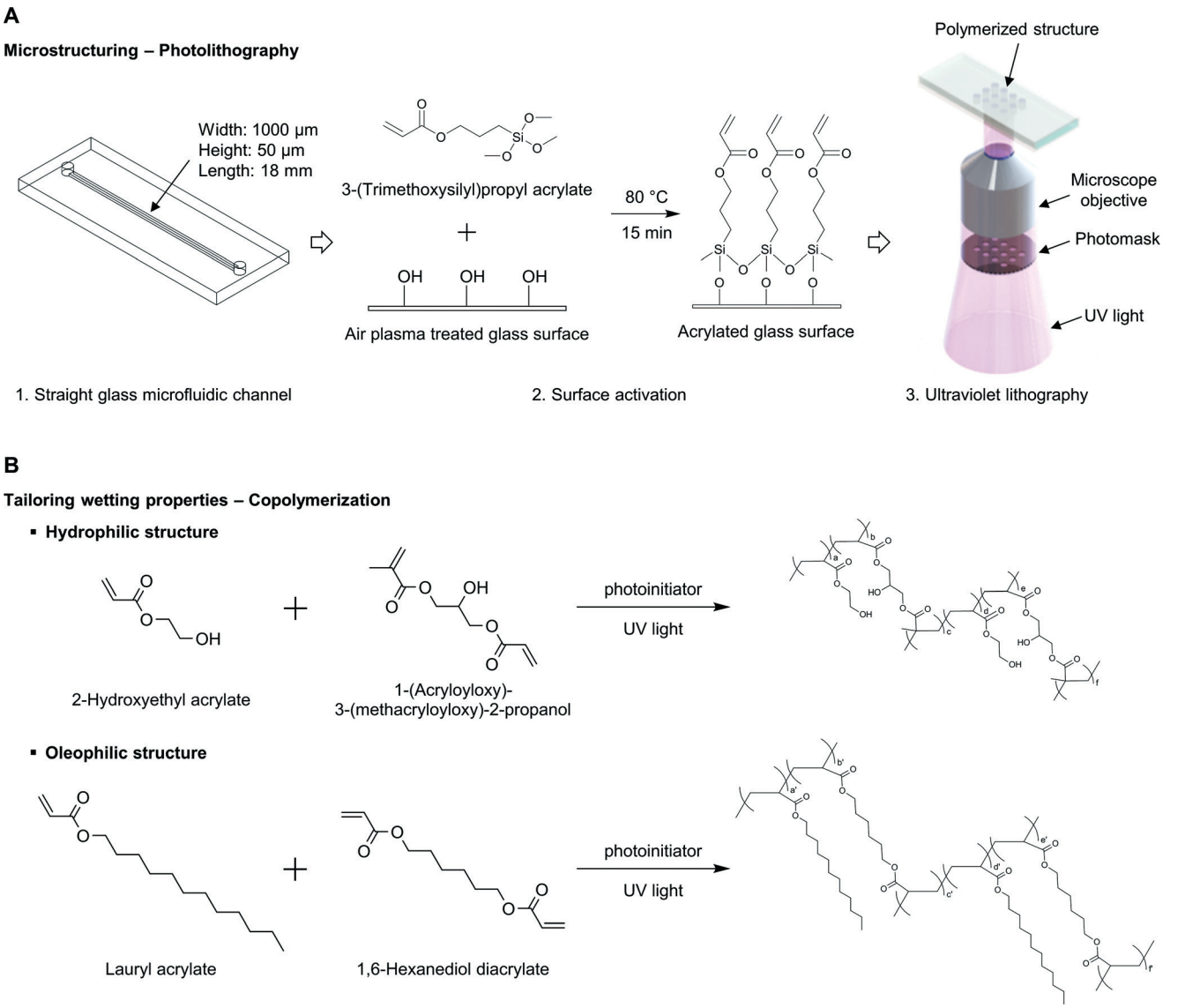

Fig. 1 Two main concepts of our approach: lithographic patterning of features and tailoring of wetting properties. (A) Schematic showing the photolithography process. Surfaces of an initially empty microchannel are activated with 3-(trimethoxysilyl)propyl acrylate for fixing polymerized structures, and then the channel is filled with a UV-curable precursor solution. A microstructure is synthesized with photomask-defined geometry by UV exposure. The uncured precursor solution is removed by flushing with acetone. (B) Hydrophilic and oleophilic microstructures are designed and built by UV-initiated copolymerization. The degree of hydrophilicity and oleophilicity is tailored by adjusting the composition of crosslinker and monomer. 3-(acryloyloxy)-2-hydroxypropyl methacrylate (AHM) and 1,6-hexanediol diacrylate (HDDA) are used as crosslinkers, and 2-hydroxyethyl acrylate (HEA) and lauryl acrylate (LA) are used as additive monomers for hydrophilic and oleophilic structures, respectively. Precursor solutions have the same concentration of photoinitiator, Darocur 1173 (2-hydroxy-2-methylpropiophenon).

hydrophobic surface is then oleophilic. A hydrophobic surface having a high water contact angle in the air does not prefer water to air; however, this does not necessarily mean that the surface will like oil than water. In other words, when the wetting property of a surface is investigated, one has to check its contact angle in the presence of the both of immiscible fluids (solid–water–oil) or has to check the water contact angle in air and the oil contact angle in air separately, and then correlate the relationship of solid–water–oil. This relationship between hydrophilic/phobic and oleophilic/phobic is clearly explained in the article of Jung and Bhushan.[23] For these reasons, in our study we measured water contact angles in decane to define the polymerized surfaces' relative preference between oil and water. Throughout this article, we use terms hydrophilic and oleophilic expressing a solid surface's behavior of water-like and oil-like, respectively, in the presence of oil and water.

Our approach to tailoring the wetting property of polymeric structures is through tuning the ratio of hydrophilic and oleophilic components. Here, we use polymeric crosslinkers that have reactive vinyl groups, which can polymerize with photoinitiator, 2-hydroxy-2-methylpropiophenon (Darocur 1173, Sigma-Aldrich), upon exposure to the ultraviolet light. We choose hydrophilic and oleophilic crosslinking

Open Access Article. Published on 09 June 2015. Downloaded on 7/25/2025 4:28:56 AM.
This article is licensed under a Creative Commons Attribution-NonCommercial 3.0 Unported Licence.

Table 1 Chemical compositions of the copolymerized hydrophilic and oleophilic structures (v/v%)

Hydrophilic						Oleophilic					
	H-1	H-2	H-3	H-4	H-5		O-1	O-2	O-3	O-4	O-5
1-(Acryloyloxy)-3-(methacryloyloxy)-2-propanol	15%	35%	55%	75%	95%	1,6-Hexanediol diacrylate	15%	35%	55%	75%	95%
2-Hydroxyethyl acrylate	80%	60%	40%	20%	0%	Lauryl acrylate	80%	60%	40%	20%	0%
Darocur 1173	5%	5%	5%	5%	5%	Darocur 1173	5%	5%	5%	5%	5%

agents, 1-(acryloyloxy)-3-(methacryloyloxy)-2-propanol (AMP) (Polysciences, Inc.) and 1,6-hexanediol diacrylate (HDDA) (Sigma-Aldrich), respectively, that can confer chemical and physical robustness. The desired wetting property is further increased by copolymerization with additives, hydrophilic and oleophilic monomers, 2-hydroxyethyl acrylate (HEA) (Sigma-Aldrich) and lauryl acrylate (LA) (Sigma-Aldrich) (Fig. 1B, Table 1).

3 Result and discussion

3.1 Water contact angle measurement in decane

Hydrophilic and oleophilic substrates with controlled crosslinker-monomer volume–volume percent concentration were prepared by pressing a drop of the precursor solution on an acrylated glass. The solution was pressed with another glass slide, and then it was cured under the UV (365 nm) lamp for 3 minutes. The water contact angle on the substrate was measured in a quartz cell which is filled with decane using a goniometer (Rame-Hart). Each measurement of advancing and receding contact angles of water in decane was repeated three times. More details of the contact angle measurement process is described in ESI†.

Fig. 2 shows the trend of water contact angles in decane with respect to crosslinker-monomer volume–volume percent concentration of hydrophilic and oleophilic precursors (Table 1). We modulated the wetting properties of substrates from hydrophilic to oleophilic in a continuous range ($\theta_{adv_{water\ in\ oil}}$ from 60° to 144°) by tuning the ratio of components. As the portion of the hydrophilic or oleophilic additive (HEA or LA) increased, the hydroxyl or hydrocarbon of content of the polymer surfaces showed stronger interactions with polar (water) and nonpolar (decane) phases, that decreased and increased the water contact angle, respectively.

As the ratio of hydrophilic or oleophilic functionalities increase, contact angle hysteresis, the difference between advancing and receding contact angles, is also increased (H-5 → H-1, O-5 → O-1). This contact angle hysteresis increase is most likely due to the change of crosslinking density, as mentioned in as previous studies that investigated contact angles on polymer surfaces.[50–52] Less crosslinked polymeric surfaces are facile to rearrange their chemical structure upon the wetting of solvent, and thus allow the solvent penetration. However, highly crosslinked surfaces inhibit this restructuring by constrained chain mobility, and the solvent is unable to penetrate. As a result, the surfaces of lower crosslinking density have the larger difference of the surface energy for the polar and nonpolar solvents wetting, consequently show higher contact angle hysteresis.[51]

3.2 Immiscible fluid displacement – single post

After polymerization of microstructures in empty microchannels and thoroughly rinsing uncured precursor solutions with acetone, subsequent flow experiments were conducted (Fig. 3). The micromodel was then filled with decane, and water displaced decane under constant applied pressure (Fig. 4A). Experiments with a reversed flow sequence were also performed (Fig. 4B). A movie and sequentially captured images showing the displacement process for the oleophilic post (O-1) is available as ESI.†

Since the oleophilic posts (O-1, O-5) prefer oil to water, the oleophilic post formed a thin oil layer between the posts and water. The most oleophilic post (O-1) was eventually encapsulated by oil in the case of oil → water flow, while the hydrophilic posts (H-1, H-5) left water at the posterior area in the case of water → oil flow. In the opposite flow sequence for each post, water/oil was repelled by oleophilic/hydrophilic

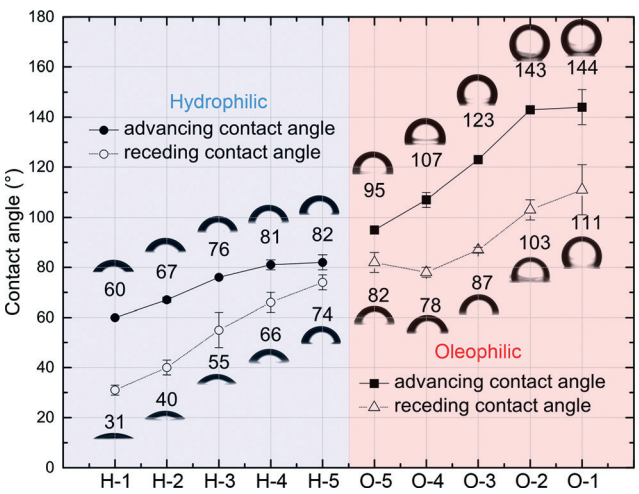

Fig. 2 Water contact angles in decane. Hydrophilic (H-1–5) and oleophilic (O-1–5) substrates with controlled composition were prepared and the substrates immersed in decane to measure advancing and receding water contact angles. As the ratio of hydrophilic and oleophilic additive monomers in precursor solution increases, hydrophilicity and oleophilicity increases (H-5 → H-1 and O-5 → O-1), and the contact angle hysteresis increases as well due to the decrease in crosslinking density. Water contact angles in decane on pure glass (θ_{adv} = 19°, θ_{rec} = 0°) and acrylate treated glass (θ_{adv} = 58°, θ_{rec} = 35°) were also measured for reference.

This journal is © The Royal Society of Chemistry 2015

Open Access Article. Published on 09 June 2015. Downloaded on 7/25/2025 4:28:56 AM.
This article is licensed under a Creative Commons Attribution-NonCommercial 3.0 Unported Licence.

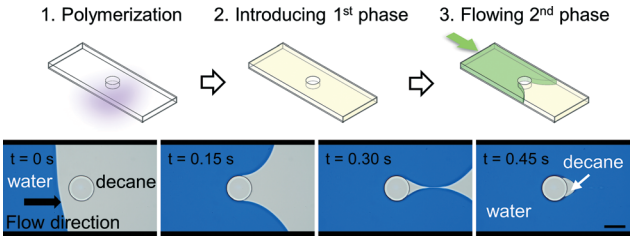

Fig. 3 Single post oil–water displacement experiments. After building a single post in a microchannel and rinsing the channel with acetone to remove any uncured precursor solution, two immiscible fluids were serially introduced into the channel (decane followed by water). Scale bar is 100 μm.

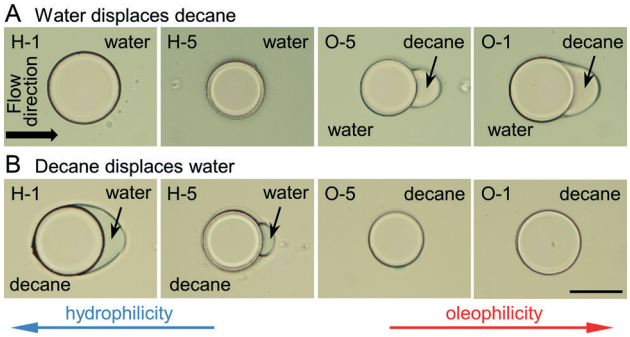

Fig. 4 (A) Microchannels were first filled with decane, and then water was introduced into the channels (flow direction from the left to the right). The alphanumeric code refers to the copolymer compositions listed in Table 1, H-1 being the most hydrophilic and O-1 the most oleophilic. Water can completely displace decane for the hydrophilic post systems (H-1, H-5), while decane remains entrained by the oleophilic posts (O-5, O-1). The most oleophilic post (O-1) is completely encapsulated by decane, while the less oleophilic post (O-5) has a well-defined droplet adhered to the downstream side. (B) Flow sequence is reversed relative to (A): the channels were filled with water, and then water was displaced by decane. Similar to the previous displacement, the most hydrophilic post (H-1) was entirely surrounded by water, H-5 was partially covered with water, and no water reamained around the oleophilic posts. Scale bar is 100 μm.

posts since the posts prefer the displacing phase to displaced phase. Computational simulation of the fluid displacement for single posts was performed in OpenFOAM 2.3.0 and the results are available as ESI.†

Based on these initial experiment sets, we can construct a set of eight possible experimental combinations: four posts of different wetting preferences and two flow sequences (oil → water, water → oil) (Fig. 4). These eight combinations can be used to demonstrate typical underground reservoir scenarios: the drainage process (when a non-wetting entering fluid displaces a wetting fluid) and the imbibition process (when a wetting fluid displaces a non-wetting fluid).

Four posts in Fig. 4 were photopatterned with the same photomask, thus right after polymerization all four posts had the same diameters. However, there were slight size changes at different solvent conditions. There was no significant size changes with homogeneous hydrophilic (H-5, AMP 95%, photoinitiator 5%) and oleophilic (O-5, HDDA 95%, photoinitiator 5%) posts. On the other hand, the most hydrophilic (H-1, AMP 15%, HEA 80%, photoinitiator 5%) and oleophilic (O-1, HDDA 15%, LA 80%, photoinitiator 5%) posts showed different sizes at different solvent conditions (acetone, water, and decane). This different swelling behavior can be explained with the same reason of previous contact angle hysteresis trend, the crosslinking density and the affinity of hydrophilic/oleophilic posts for polar/nonpolar solvents.[51–55] In comparison with H-5 or O-5, H-1 and O-1 had relatively lower crosslinker and higher hydrophilc/oleophilic monomer concentrations. As a result, the higher molecular chain mobility and the larger mesh size increased restructuring ability and allowed polar/nonpolar solvent penetration, thus the posts were swelled. The post size changes in different solvents was investigated, and the result is shown in the accompanying ESI.†

3.3 Multi-post micromodel with heterogeneous wettability

The first multi-post micromodel was created by polymerizing multiple posts one by one. The hydrophilic posts had been created, and the channel was rinsed, then the oleophilic posts were polymerized with the same photomask (Fig. 5). Immiscible fluids were sequentially injected into the channel at constant pressures (water → decane → fluorinated oil, FC-40; immiscible to both water and decane).

Decane (dyed with an oil dye, Oil Red O (Sigma-Aldrich)), was held on the oleophilic post (red-stained with the oil dye), and water was captured on the hydrophilic post (Fig. 5A). Water and decane pathways were formed in parallel following each set of three hydrophilic and oleophilic posts (Fig. 5B), and a V-shape water reservoir was made (Fig. 5C). A square shaped water reservoir was isolated from the FC-40 and was surrounded by decane (Fig. 5D). Because the hydrophilic and oleophilic posts were already occupied with their preferred phases, FC-40 was not able to displace the decane and water being entrained by the posts.

The second multi-post micromodel was constructed with a photomask having multiple geometric features, in this case a 3 × 5 array of circles. We made separate hydrophilic (H-1) and oleophilic (O-1) areas with two different precursors. After thoroughly rinsing with acetone, the microchannel was first filled with decane, displaced by water from the left to the right, and displaced again by decane from the right to the left to see different behaviors (Fig. 6). From the first displacement image, we can see that decane was fully displaced by water in the hydrophilic region while water was not able to penetrate through the oleophilic region (Fig. 6-1). To confirm the hydrophilicity of the upper half, decane was re-introduced from the right side of the image, and it is clearly shown that hydrophilic posts were connected by water along the direction of the flow (Fig. 6-2).

The third multi-post micromodel had three different regions of wetting. The ability to tune wettability in a continuous manner is one of the advantages of our approach compared with other methods. Typically other wettability

Open Access Article. Published on 09 June 2015. Downloaded on 7/25/2025 4:28:56 AM.
This article is licensed under a Creative Commons Attribution-NonCommercial 3.0 Unported Licence.

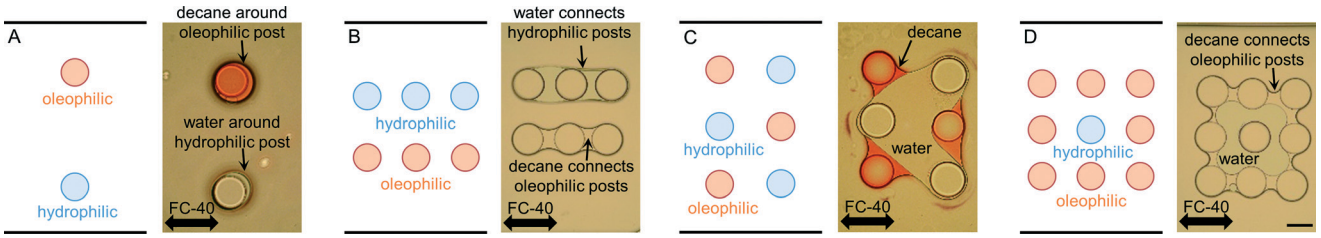

Fig. 5 Demonstration of mixed wettability micromodels. Hydrophilic (H-1) and oleophilic (O-1) posts were built together in the same microchannel by successive microstructuring processes, having a rinsing step between the two polymerization steps. The position, arrangement, and shape of the posts can be arbitrarily determined with the microscope stage control and the photomask design. Immiscible fluids were injected into the channels (water → decane → fluorinated oil (FC-40)). The hydrophilic and oleophilic posts show the same wetting behavior for water and oil as shown in the previous single-post micromodels. The figure shows four different examples of multi-post experiment. (A) A pair of hydrophilic and oleophilic posts. Decane was dyed with an oil dye, Oil Red O, for visualization, and oleophilic post was stained with the oil dye. (B) Each of three serial hydrophilic and oleophilic posts in parallel. (C) Zigzag configuration of hydrophilic and oleophilic posts. (D) One hydrophilic post forming a water pocket at the channel center, surrounded by decane that inhibits the contact between water and FC-40. Scale bar is 100 mm.

modification methods can achieve only binary behavior (mostly hydrophilic or hydrophobic). Three different precursors were used to create three different wetting regions (hydrophilic (H-1), oleophilic (O-1), and intermediate (O-5)), and decane and water were introduced into the micromodel (Fig. 7). After decane displacement by water, all of 9 oleophilic posts (O-1) held decane while decane was totally displaced by water at all of the 40 hydrophilic posts (H-1). Around 9 intermediate posts (O-5) out of 14 retained decane around them after water flooding. When decane was re-introduced, the opposite result was obtained: none of the 9 oleophilic posts (O-1) held water, and all of the 40 hydrophilic posts (H-1) formed a water film around which isolated them from decane. Around 3 intermediate posts (O-5) were wetted by the displaced water. These trends are expected based on the results of previously described single post experiment. For the multi-post microfluidic channel used in Fig. 7, we repeated the same decane/water displacement experiments 4 times with the same device, and observed that the oleophilic (O-1) and hydrophilic posts (H-1) always showed the same result of totally wetting and totally non-wetting with respect to their preferred and unpreferred phases (Fig. 8, Table 2).

Based on the above three experiments, it is possible to have insight into how the porosity (the fraction of void space) and the wettability (the relative preference of solid phase for fluid phases) influence the displacement process. It is well known by Darcy's law that the lower the porosity, the lower the permeability. However, as can be seen through the above experiments, we can infer that even for the same porosity, the drainage process requires higher pressure than the imbibition process. During the drainage process (when most of the posts prefer the displaced phase to the displacing phase), the higher pressure is needed to displace the wetting phase. On the other hand, during the imbibition process (when the posts prefer the displacing phase to the displaced phase), the non-wetting phase is easily displaceable since the posts prefer the displacing phase to the displaced phase. In other words, wettability plays a role in immiscible displacement as important as the porosity does. Moreover, the influence of wettability may increase as effective surface area increases, such as the case of smaller posts having the same porosity. With further experiments using multi-post micromodels, we can broaden our understanding of how the geometric and the chemical properties of a micromodel are correlated to and affect the displacement process.

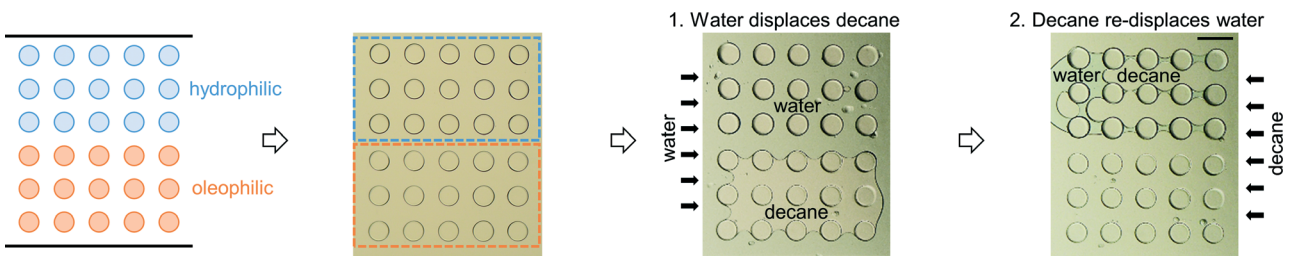

Fig. 6 Micromodel with hydrophilic (H-1) and oleophilic (O-1) sub-regions. Hydrophilic and oleophilic areas were defined in a microchannel with multiple posts. The method of microstructuring is different from the first multi-post micromodels. First, multiple posts (3 × 5) for the upper-half hydrophilic area was polymerized by a single UV exposure with a mask having 3 × 5 arrays of 15 circles. After rinsing the channel to remove the uncured precursor, the lower-half oleophilic area was made in the same way. The hydrophilic and oleophilic regions were made with only two UV lightings as broad as the scope of UV illumination. With this micromodel, decane → water → decane flow experiment was conducted. When water displaced decane, decane was selectively left in the oleophilic area while decane in the hydrophilic area was entirely washed away. Decane was re-introduced from the right to the left for the purpose of checking the hydrophilicity of the upper half, and the rows of hydrophilic posts were connected by water. Scale bar is 200 mm.

This journal is © The Royal Society of Chemistry 2015

Open Access Article. Published on 09 June 2015. Downloaded on 7/25/2025 4:28:56 AM.
This article is licensed under a Creative Commons Attribution-NonCommercial 3.0 Unported Licence.

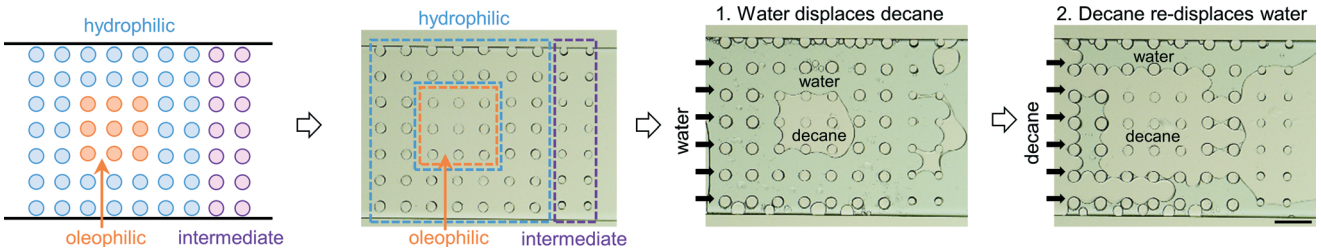

Fig. 7 Heterogeneous wettability micromodel with three types of wetting behavior (hydrophilic (H-1), oleophilic (O-1), and intermediate (O-5)) were created in a single microchannel. Since the microchannel had three different wetting behaviors, three different precursor solutions had to be introduced into the channel. After three continuous microstructuring, an immiscible displacement experiment was carried out in the order decane → water → decane. When water displaced decane, oil reservoir built up around the oleophilic posts at the center while some of the intermediate posts at the downstream area held decane. Decane was re-introduced from the left, and only few pathways of decane were formed through hydrophilic posts. Scale bar is 200 mm.

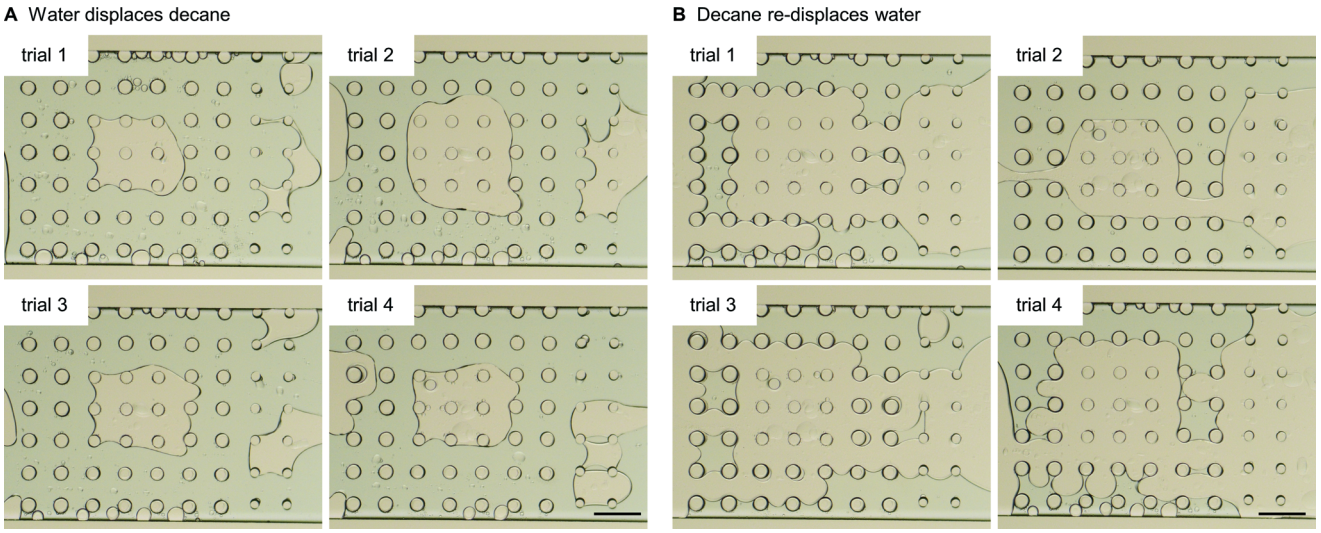

Fig. 8 For the same multi-post microfluidic channel used in Fig. 7, we repeated the same decane/water displacement experiments, and counted how many posts held the displaced phase after the other phase was introduced. Images after (A) water displaces decane, and (B) decane re-displaces water. Scale bar is 200 mm.

Table 2 Number of posts holding the displaced phase after flushing with an immiscible fluid. Data in this table refer to experiments shown in Fig. 8

	A Posts holding decane after water displaces decane					B Posts holding water after decane re-displaces water				
	Trial 1	Trial 2	Trial 3	Trial 4	Average	Trial 1	Trial 2	Trial 3	Trial 4	Average
Oleophilic	9/9 (100%)	9/9 (100%)	9/9 (100%)	9/9 (100%)	9/9 (100%)	0/9 (0%)	0/9 (0%)	0/9 (0%)	0/9 (0%)	0/9 (0%)
Hydrophilic	0/40 (0%)	0/40 (0%)	0/40 (0%)	0/40 (0%)	0/40 (0%)	40/40 (100%)	40/40 (100%)	40/40 (100%)	40/40 (100%)	40/40 (100%)
Intermediate	9/14 (64%)	10/14 (71%)	8/14 (57%)	10/14 (71%)	9.25/14 (66%)	3/14 (21%)	5/14 (36%)	7/14 (50%)	1/14 (7%)	4/14 (29%)

4 Conclusions

In this study, we have introduced a new on-demand micromodel fabrication technique with tailored wetting properties. Unlike conventional soft lithography, our approach does not require a master silicon wafer to be prepared in a clean room, nor does it require significant time and effort to fabricate different porous geometries and to modify wetting properties of the micromodels. Geometric features, such as the shape, size, and distance between microstructures can be controlled for micromodel design optimization or systematical study of their effects. At the same time, each

Open Access Article. Published on 09 June 2015. Downloaded on 7/25/2025 4:28:56 AM.
This article is licensed under a Creative Commons Attribution-NonCommercial 3.0 Unported Licence.

structure can have a different wetting property over a continuous range that is pre-formulated, without additional surface modification steps. This is the first method which can simultaneously create and tailor the wettability of a microstructure in a fluidic device. We demonstrated experiments on immiscible fluid displacement with single posts. We also demonstrated oil–water displacement studies in devices with spatially varying wetting properties. Like real reservoir formations, we can mimic locally oleophilic niches within an otherwise hydrophilic channel. To the best of our knowledge, this is also the first micromodel that has more than a binary wettability within it.

Micromodels have broadened our understanding of multiphase flow in porous media and have provided solutions for practical engineering issues by visualizing phenomena occurring in subsurface oil reservoirs. However, multi-phase flow mechanisms at the pore scale are still not clearly explainable, and newly developed practices or functional materials need repeated experiments before applying them at production sites. In this context, the micromodel fabrication method demonstrated in this article can be used for rapid prototyping. To understand fundamental physics of underground flows, it is more desirable to start with a micromodel that has simple and prescribed structures, rather than injecting immiscible fluids into the black-box micromodel that has complex geometries and undefined wettability. New production practices and materials can be tested within well-defined micromodels that can represent various types of oil reservoirs.

In addition to the oil-reservoir studies, this fabrication method can be utilized for other applications in microfluidics. For example, one can use our method to rapidly prototype pillar arrangements within a flow device that can then be used to sculpt complex chemical patterns.[56] The controlled wetting within a device can be useful to stabilize fluid-fluid interfaces as particles are pulled across them by magnetic forces for separations.[57] Internal features with controlled wetting will also be useful in capillary guided wetting processes[58] for assembly of cells and organ on chip devices. From the technical side, the microfluidic device production can be improved by a stand-alone, photopatterning setup which has a broader UV lithography area or by a microscope with an automated positioning stage for a precisely controlled configuration of microstructures.

Acknowledgements

We acknowledge Ankur Gupta for help on the computational simulation. This work was supported by funding from Saudi Aramco and the NSF grants DMR-1006147 and CMMI-1120724.

References

1 C. C. Mattax and J. R. Kyte, *Soc. Pet. Eng. J.*, 1962, **2**, 177–184.
2 W. W. Owens and D. L. Archer, *J. Pet. Technol.*, 1971, **23**, 873–878.
3 R. A. Salathiel, *J. Pet. Technol.*, 1973, **25**, 1216–1224.
4 A. R. Kovscek, H. Wong and C. J. Radke, *AIChE J.*, 1993, **39**, 1072–1085.
5 J.-C. Perrin and S. Benson, *Transp. Porous Media*, 2010, **82**, 93–109.
6 T. Austad, S. F. Shariatpanahi, S. Strand, C. J. J. Black and K. J. Webb, *Energy Fuels*, 2012, **26**, 569–575.
7 S. C. M. Krevor, R. Pini, L. Zuo and S. M. Benson, *Water Resour. Res.*, 2012, **48**(2), DOI: 10.1029/2011WR010859.
8 N. K. Karadimitriou and S. M. Hassanizadeh, *Vadose Zone J.*, 2012, **11**(3), DOI: 10.2136/vzj2011.0072.
9 C. Tsakiroglou, O. Vizika-kavvadias and R. Lenormand, *Int. Symp. Soc. Core Anal.*, 2013, pp. 1–13.
10 D. Sinton, *Lab Chip*, 2014, **14**, 3127–3134.
11 C. U. Hatiboglu and T. Babadagli, *Phys. Rev. E: Stat., Nonlinear, Soft Matter Phys.*, 2008, **77**, 066311.
12 C. Cottin, H. Bodiguel and A. Colin, *Phys. Rev. E: Stat., Nonlinear, Soft Matter Phys.*, 2011, **84**, 026311.
13 C. Zhang, M. Oostrom, T. W. Wietsma, J. W. Grate and M. G. Warner, *Energy Fuels*, 2011, **25**, 3493–3505.
14 J. Joseph, N. Siva Kumar Gunda and S. K. Mitra, *Chem. Eng. Sci.*, 2013, **99**, 274–283.
15 K. He, L. Xu, Y. Gao, K. B. Neeves, X. Yin, B. Bai, Y. Ma and J. Smith, *Pap. SPE 169147*, 2014, pp. 12–16.
16 J. Beaumont, H. Bodiguel and A. Colin, *Soft Matter*, 2013, **9**, 10174–10185.
17 K. Ma, R. Liontas, C. A. Conn, G. J. Hirasaki and S. L. Biswal, *Soft Matter*, 2012, **8**, 10669.
18 C. A. Conn, K. Ma, G. J. Hirasaki and S. L. Biswal, *Lab Chip*, 2014, **14**, 3968–3977.
19 T. W. Haas, H. Fadaei, U. Guerrero and D. Sinton, *Lab Chip*, 2013, **13**, 3832–3839.
20 G. C. Kini, J. Yu, L. Wang, A. T. Kan, S. L. Biswal, J. M. Tour, M. B. Tomson and M. S. Wong, *Colloids Surf., A*, 2014, **443**, 492–500.
21 T. M. Okasha, J. J. Funk and H. N. Rashidi, *SPE Middle East Oil Gas Show Conf.*, 2007, pp. 1–10.
22 L. E. Treiber and W. W. Owens, *Soc. Pet. Eng. J.*, 1972, **12**, 531–540.
23 Y. C. Jung and B. Bhushan, *Langmuir*, 2009, **25**, 14165–14173.
24 M. Jin, J. Wang, X. Yao, M. Liao, Y. Zhao and L. Jiang, *Adv. Mater.*, 2011, **23**, 2861–2864.
25 A. K. Kota, G. Kwon, W. Choi, J. M. Mabry and A. Tuteja, *Nat. Commun.*, 2012, **3**, 1025.
26 N. S. K. Gunda, B. Bera, N. K. Karadimitriou, S. K. Mitra and S. M. Hassanizadeh, *Lab Chip*, 2011, **11**, 3785–3792.
27 J. W. Grate, R. T. Kelly, J. Suter and N. C. Anheier, *Lab Chip*, 2012, **12**, 4796–4801.
28 N. K. Karadimitriou, V. Joekar-Niasar, S. M. Hassanizadeh, P. J. Kleingeld and L. J. Pyrak-Nolte, *Lab Chip*, 2012, **12**, 3413–3418.
29 D. Bartolo, G. Degré, P. Nghe and V. Studer, *Lab Chip*, 2008, **8**, 274–279.

 This journal is © The Royal Society of Chemistry 2015

Open Access Article. Published on 09 June 2015. Downloaded on 7/25/2025 4:28:56 AM.
This article is licensed under a Creative Commons Attribution-NonCommercial 3.0 Unported Licence.

30 V. Berejnov, N. Djilali and D. Sinton, *Lab Chip*, 2008, **8**, 689–693.
31 M. H. Schneider and P. Tabeling, *Am. J. Appl. Sci.*, 2011, **8**, 927–932.
32 E. Sollier, C. Murray, P. Maoddi and D. Di Carlo, *Lab Chip*, 2011, **11**, 3752–3765.
33 M. Wu, F. Xiao, R. M. Johnson-Paben, S. T. Retterer, X. Yin and K. B. Neeves, *Lab Chip*, 2012, **12**, 253–261.
34 K. W. Bong, J. Xu, J.-H. Kim, S. C. Chapin, M. S. Strano, K. K. Gleason and P. S. Doyle, *Nat. Commun.*, 2012, **3**, 805.
35 P. Horgue, F. Augier, P. Duru, M. Prat and M. Quintard, *Chem. Eng. Sci.*, 2013, **102**, 335–345.
36 N. K. Karadimitriou, M. Musterd, P. J. Kleingeld, M. T. Kreutzer, S. M. Hassanizadeh and V. Joekar-Niasar, *Water Resour. Res.*, 2013, **49**, 2056–2067.
37 Q. Zhang, N. K. Karadimitriou, S. M. Hassanizadeh, P. J. Kleingeld and A. Imhof, *J. Colloid Interface Sci.*, 2013, **401**, 141–147.
38 W. Song, T. W. de Haas, H. Fadaei and D. Sinton, *Lab Chip*, 2014, **14**, 4382–4390.
39 J. W. Grate, M. G. Warner, J. W. Pittman, K. J. Dehoff, T. W. Wietsma, C. Zhang and M. Oostrom, *Water Resour. Res.*, 2013, **49**, 4724–4729.
40 B. Levaché, A. Azioune, M. Bourrel, V. Studer and D. Bartolo, *Lab Chip*, 2012, **12**, 3028–3031.
41 M. H. Schneider, H. Willaime, Y. Tran, F. Rezgui and P. Tabeling, *Anal. Chem.*, 2010, **82**, 8848–8855.
42 H. Hillborg, N. Tomczak, A. Ola, H. Scho and G. J. Vancso, *Langmuir*, 2004, **20**, 785–794.
43 A. Oláh, H. Hillborg and G. Vancso, *Appl. Surf. Sci.*, 2005, **239**, 410–423.
44 D. Dendukuri, D. C. Pregibon, J. Collins, T. A. Hatton and P. S. Doyle, *Nat. Mater.*, 2006, **5**, 365–369.
45 D. Dendukuri, S. S. Gu, D. C. Pregibon, T. A. Hatton and P. S. Doyle, *Lab Chip*, 2007, **7**, 818–828.
46 K. W. Bong, D. C. Pregibon and P. S. Doyle, *Lab Chip*, 2009, **9**, 863–866.
47 D. Dendukuri, P. Panda, R. Haghgooie, J. M. Kim, T. A. Hatton and P. S. Doyle, *Macromolecules*, 2008, **41**, 8547–8556.
48 R. L. Srinivas, S. D. Johnson and P. S. Doyle, *Anal. Chem.*, 2013, **85**, 12099–12107.
49 Z. Cheng, H. Lai, Y. Du, K. Fu, R. Hou, N. Zhang and K. Sun, *ACS Appl. Mater. Interfaces*, 2013, **5**, 11363–11370.
50 H. Yasuda, A. K. Sharma and T. Yasuda, *J. Polym. Sci., Polym. Phys. Ed.*, 1981, **19**, 1285–1291.
51 D. L. Schmidt, R. F. Brady, K. Lam, D. C. Schmidt and M. K. Chaudhury, *Langmuir*, 2004, **20**, 2830–2836.
52 J. C. Yarbrough, J. P. Rolland, J. M. Desimone, M. E. Callow, J. A. Finlay and J. A. Callow, *Macromolecules*, 2006, **39**, 2521–2528.
53 S. J. Kim, S. J. Park and S. I. Kim, *React. Funct. Polym.*, 2003, **55**, 53–59.
54 D. K. Hwang, J. Oakey, M. Toner, J. A. Arthur, K. S. Anseth, S. Lee, A. Zeiger, K. J. V. Vliet and P. S. Doyle, *J. Am. Chem. Soc.*, 2009, **131**, 4499–4504.
55 Y. Diao, K. E. Whaley, M. E. Helgeson, M. A. Woldeyes, P. S. Doyle, A. S. Myerson, T. A. Hatton and B. L. Trout, *J. Am. Chem. Soc.*, 2012, **134**, 673–684.
56 H. Amini, E. Sollier, M. Masaeli, Y. Xie, B. Ganapathysubramanian, H. A. Stone and D. Di Carlo, *Nat. Commun.*, 2013, **4**, 1826.
57 S. S. H. Tsai, J. S. Wexler, J. Wan and H. A. Stone, *Appl. Phys. Lett.*, 2011, **99**, 19–22.
58 M. Kang, W. Park, S. Na, S.-M. Paik, H. Lee, J. W. Park, H.-Y. Kim and N. L. Jeon, *Small*, 2015, **11**, 2789–2797.